Mechanism of Wireless Power Transfer System Waveform Distortion Caused by Nonideal Gallium Nitride Transistor Characteristics*

Shaoyu Sun[1, 2], *Jianshan Zhang*[2], *Wengang Wu*[2], *Ling Xia*[3*] *and Yufeng Jin*[1, 2]

(1. Shenzhen Graduate School, Peking University, Shenzhen 518055, China;
2. Institute of Microelectronics, Peking University, Beijing 100871, China;
3. Shenzhen Hai Li Tech., Inc., Shenzhen 518129, China)

Abstract: Gallium nitride (GaN) field-effect transistors have low ON resistance and switching losses in high-frequency (>MHz) resonant wireless power transfer systems. Nevertheless, their performance in the system is determined by their characteristics and operation mode. A particular operating mode in a 6.78-MHz magnetic resonant wireless transfer system that employs class-D GaN power amplifiers in the zero-voltage switching mode is studied. Two operation modes, the forward mode and the reverse mode, are investigated. The nonideal effect under the device-level dynamic resistance and thermal effect are also analyzed. The dynamic resistance under different operation modes is demonstrated to have different generation mechanisms. Finally, the device characteristics with system operating conditions are combined, and the effects of temperature and dynamic resistance under different operating conditions are evaluated.

Keywords: GaN, wireless power transfer, dynamic resistance, thermal effect

1 Introduction

Wireless power transfer (WPT) is recognized as an efficient and resourceful technology for wireless charging in radio frequency identification, electric vehicles, buried sensors, portable electronic devices, and medical devices [1-2]. Near-field WPT systems have a high power-conversion efficiency and are widely used in short- and mid-range applications. There are two categories of near-field WPT systems: the inductive and capacitive coupling technique for short-range applications (Wireless Power Consortium standard and Power Matters Alliance standard) [3] and the magnetic resonance coupling technique for mid-range applications (AirFuel standard) [4].

Wireless power can be transferred with an operating frequency in the megahertz region via the AirFuel standard (A4WP), for example, 6.78 MHz. Owing to its high operating frequency, this standard has greater requirements in terms of device characteristics. However, the fundamental limitations and device structure of silicon with its relatively narrow bandgap make it challenging to use this material to handle high-power and high-frequency applications.

Gallium-nitride based high-electron-mobility transistors (HEMTs) have tremendous potential for high-power, high-frequency, and high-efficiency power switching applications owing to the outstanding properties of the gallium nitride (GaN) material (e.g., wide bandgap, high-electron saturation velocity, and large breakdown electric field) [5-8]. Many scholars have studied and reported on the properties of GaN field-effect transistors (FETs) at the device level. The doping, structure, and material quality can all be adjusted to improve the device characteristics. However, the device characteristic presentation in a real system is also related to circuit design and operation mode.

Manuscript received July 28, 2020; revised November 19, 2020; accepted January 6, 2021. Date of publication June 30, 2021; date of current version June 7, 2021.
* Corresponding Author, E-mail: 1005820199@qq.com
* Supported by the TSV 3D Integrate Micro/Nanosystem Lab (ZDSYS201802061805105), the Natural Science Foundation of Shenzhen (JCYJ20190808155007550), and Shenzhen Science Plan (JSGG20180504170016884).
Digital Object Identifier: 10.23919/CJEE.2021.000016

Pulsed current-voltage (I-V) measurements are widely used to research device characteristics. They can be used to describe the trap response and extract the activation energy of the deep level. However, using such measurements does not capture device behavior in realistic switching conditions [9]. Several questions arise: Do the special operation modes affect the device's characteristics in a real circuit? Does a particular circuit topology enhance or suppress the nonideal effects of a GaN FET?

At present, the application of GaN devices in practical circuits is little known. Most applications of GaN FETs operate in the forward mode (see Fig. 1a). Some devices operate in the reverse mode (see Fig. 1b), such as for synchronous rectification [10]. One characteristic that has drawn the most attention is the change in the ON resistance (R_{on}) of a GaN FET during circuit operation. R_{on} does not remain constant throughout the circuit operation. It changes with the biasing condition and operation time scale. Generally, an increase in R_{on} increases the power loss or reduces the reliability of the GaN FET [11]. Therefore, the so-called dynamic R_{on} has been extensively studied from the transistor perspective.

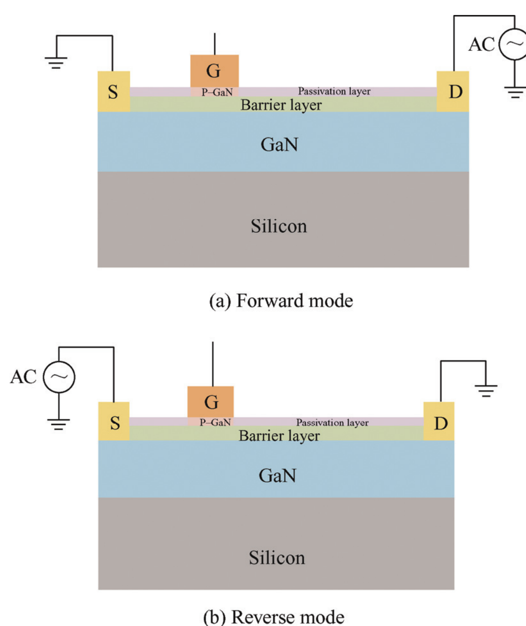

Fig. 1 Two different operation modes for a GaN device

In this work, we used an accurate measurement method to detect the value of R_{on} of the device in an WPT system operating at 6.78 MHz, as detailed in Section 2. In Section 3, a particular operation mode is investigated in the WPT system. Two nonideal effects, dynamic resistance (Section 4) and the thermal effect (Section 5) at the device level are investigated. In Section 6, we evaluate the influence of nonideal effects on the device in the WPT system, and Section 7 concludes the paper.

2 Test method

Determining the exact R_{on} requires obtaining an accurate current measurement. A new measurement setup is introduced to measure R_{on}. It involves sensing the voltage (V_{DS}) and current (I_{DS}) of a GaN FET in a circuit in real-time operation. Given the fast switching speed of a GaN device (e.g., an EPC2107 transistor), a high-bandwidth accurate current testing measurement is preferred. Four kinds of test methods are compared in Fig. 2.

Fig. 2a shows a schematic of the method using a current clamp. However, its large size and narrow bandwidth (200 MHz) severely limit its application in high-frequency testing. Moreover, based on the principle of electromagnetic coupling, the measurement results are easily affected by the position of the testing circuit.

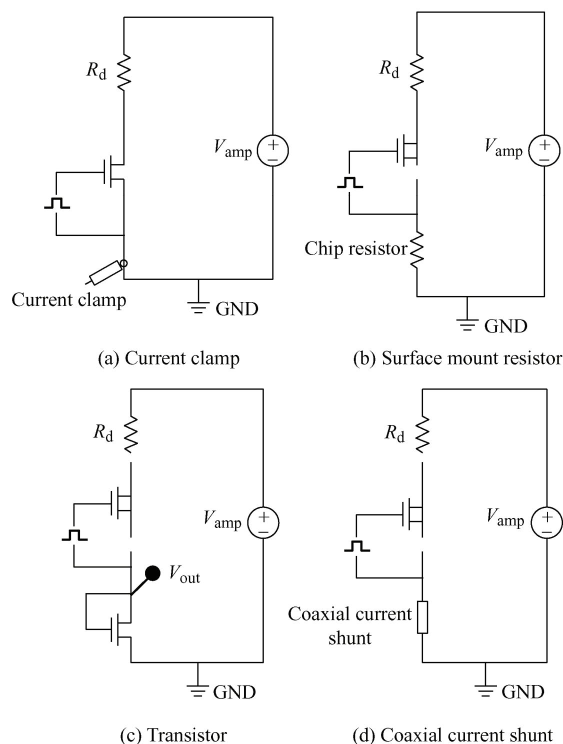

Fig. 2 Schematics of detecting current circuit

Fig. 2b shows a schematic of the method using a surface mount resistor [12]. The current is obtained by detecting the voltage on the surface mount resistor.

The main issue here is the parasitic inductance, which is mainly coming from the packaging Fig. 3a shows the test result. The surface mount resistor is 0.2 Ω. The current curve exhibits considerable oscillation. Increasing the value of the surface mount resistor can reduce the amount of oscillation, but it could affect the operation state of the device.

Fig. 2c shows a schematic of the method using a GaN transistor (in which the gate connects to the drain) to detect the current. It has a very small size and parasitic inductance. Fig. 3b shows the measurement result. When the device turns on, V_{out} does not oscillate. However, when the device turns off, V_{out} overshoots negatively. We consider that the parasitic capacitive (C_{gs}) of the device (see the inset figure) is the reason for this phenomenon. The voltage-on capacitance cannot be altered. When the device suddenly turns off, C_{gs} cannot discharge through the underlying transistor rapidly, which causes the negative overshoot. Reducing the test frequency eliminates the negative overshoot. To get an accurate R_{on}, an accurate *I-V* characteristic is also needed at high-frequency operation. This poses another challenge.

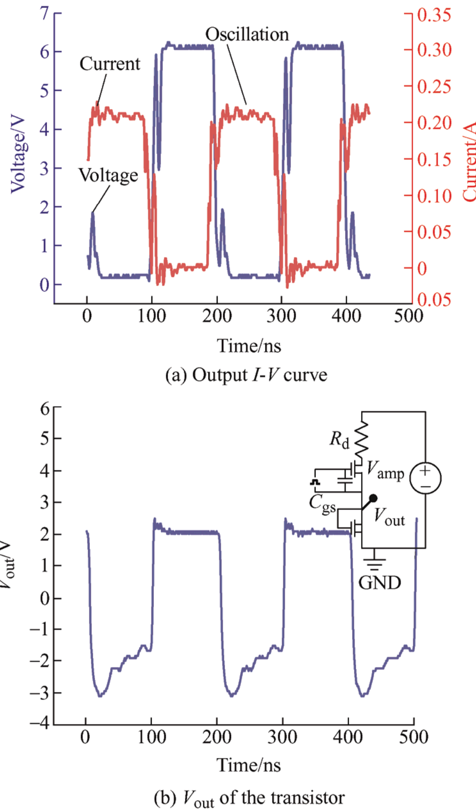

(a) Output *I-V* curve

(b) V_{out} of the transistor

Fig. 3 Measurement results using a surface mount resistor and a transistor

The most suitable method is to use a coaxial current shunt, as shown in Fig. 2d. The coaxial current shunt can be used to detect current flowing through itself and hence the GaN FET in real time (Fig. 4). The part we used was an SSDN-10 manufactured by T&M Research Products, Inc. It has accurate resistance (within 0.1 Ω), small parasitic inductance, and high bandwidth (2 GHz) [13]. We can achieve accurate $R_{on} = V_{DS}/I_{DS}$ measurements, similar to what can be achieved by using expensive commercial equipment (e.g., a Keysight B1505A).

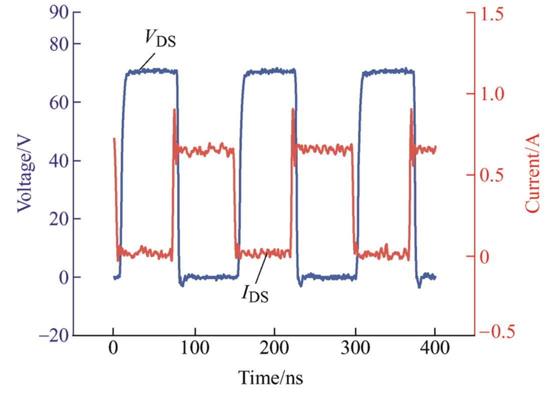

Fig. 4 Test results using a coaxial current shunt when V_{amp} = 70 V

3 Particular operation mode in a WPT system

The system level measurement was performed with a WPT module using a class-D amplifier [14] at 6.78 MHz under zero-voltage switching operation. Two EPC2107 GaN FETs were used to form a half-bridge. Fig. 5 shows a simplified schematic and an image of the WPT system. The value of R_{on} of the low-side GaN FET (Q_2) was measured. To simplify the experiment, we used a resistance (R_{load} in Fig. 5a) instead of the receiver.

Fig. 6a shows the output curve of a GaN FET in an operating system. The value of V_{GS} was set to 5 V (based on the vendor recommendation). The waveform distortion has been reported in Ref. [15]. To ensure an accurate R_{on}, we selected the average value of the middle part (in the box) as the result in Fig. 6b.

In Fig. 6a, it is worth noting the two overshoots that appear when the device switches instantaneously. The negative overshoot makes Q_2 operate in reserve mode and the positive overshoot makes Q_1 operate in reverse mode. Meanwhile, the voltage spike of the positive overshoot is higher than that of the negative

overshoot.

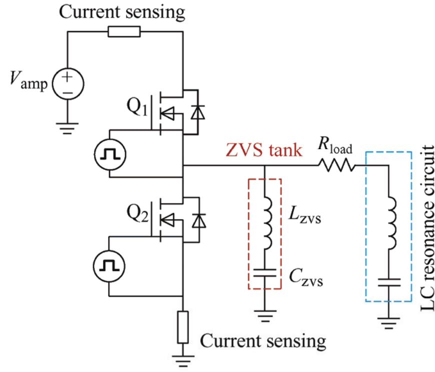

(a) Simplified cicuit diagram of the GaN half-bridge circuit

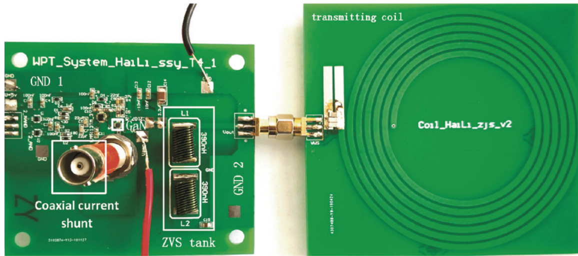

(b) R_{on} test circuit

Fig. 5 Our WPT system

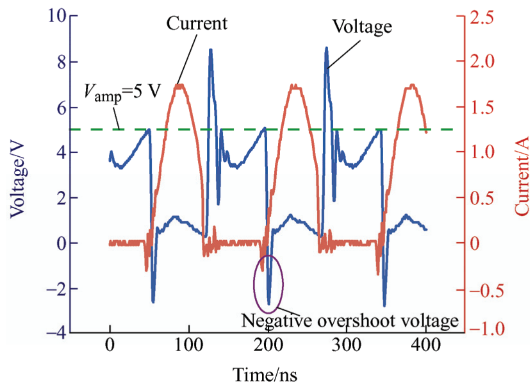

(a) V_{DS} and I_{DS} for Q2 in a real WPT system

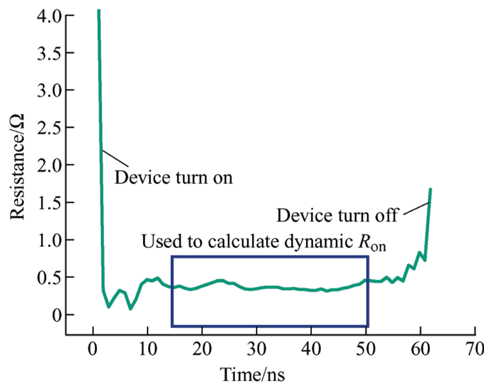

(b) GaN EET R_{on} obtained by averaging the data in the box

Fig. 6 Test results for a GaN FET operating in a WPT system

The same phenomenon was discovered by simulation using LTspice software (Fig. 7a). Fig. 7b shows a schematic of the overshoot generation.

As Q_2 turns on and Q_1 turns off, the LC resonance circuit will discharge through Q_2. The presence of dead time in the circuit and current through the inductance (coil) must be continuous. When Q_2 turns off and Q_1 has not turned on (dead time), the voltage makes Q_1 work in reverse mode (Fig. 7b, condition I). When Q_1 turns off and Q_2 does not yet turn on, the negative overshoot makes Q_2 work in reverse mode (Fig. 7b, condition Ⅱ).

In Fig. 7b, the two conditions explain the reason for the overshoot. For condition I, current flows through R_{load}, Q_1, and the power source (V_{amp}). For condition Ⅱ, current flows through Q_2 and R_{load}. Normally, the power source has internal resistance. The value of the resistance for condition I is higher than that for condition Ⅱ. We conclude that this difference is the reason for the different voltage spikes.

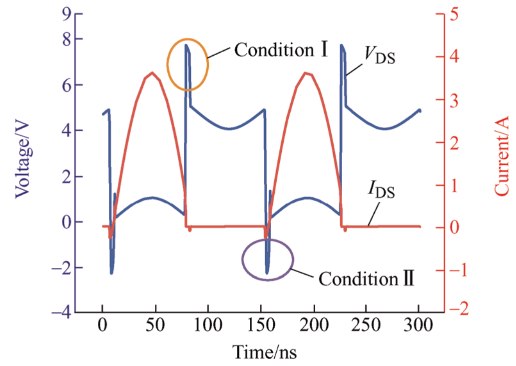

(a) Simulation using LTspice

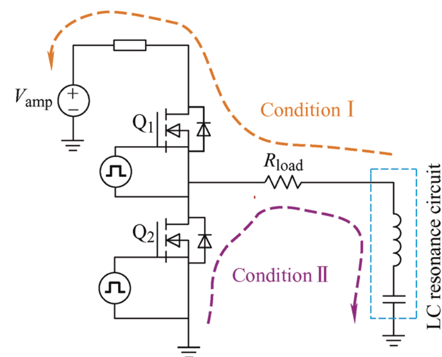

(b) Schematic of overshoot voltage generation

Fig. 7 Simulation of the device operating in a WPT system (6.78 MHz) when V_{amp} is 5 V

4 Dynamic R_{on} test

Two operation modes are presented in Section 3: forward mode and reverse mode. To more easily understand these modes, we study them in the hard-switching mode. By changing the different working conditions (such as frequency, V_{GS}, and V_{DS}),

we can observe the variation in dynamic R_{on}.

4.1 Forward mode

Fig. 8 shows the test schematic in the forward mode, and Fig. 9 shows the relationship between R_{on} and I_{DS} under different V_{GS} values. The current I_{DS} was controlled by R_{load}.

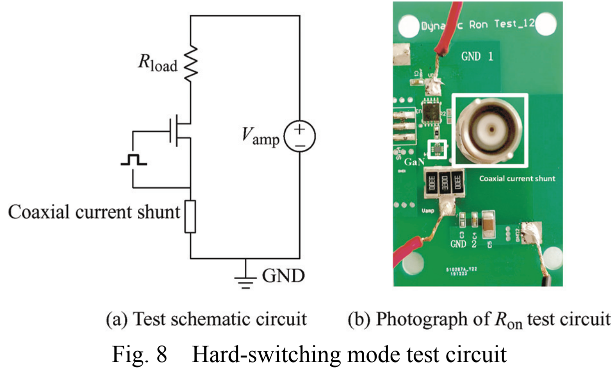

(a) Test schematic circuit (b) Photograph of R_{on} test circuit

Fig. 8 Hard-switching mode test circuit

In Fig. 9, one can observe that R_{on} is strongly dependent on I_{DS} and V_{GS}. To avoid the influence of these two factors, we set I_{DS} to 0.25 A by adjusting R_{load} and sending a few pulse signals to the gate during the test to reduce the effect of heating.

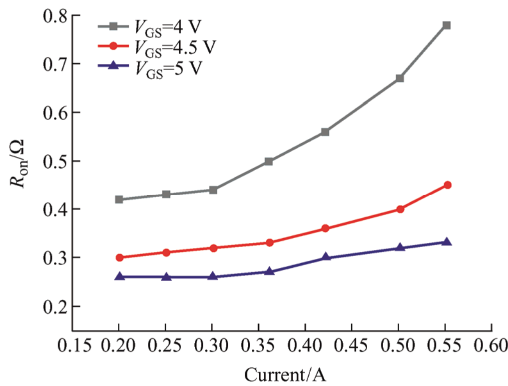

Fig. 9 R_{on} at different V_{GS} and I_{DS} values under dynamic conditions (6.78 MHz) (V_{amp} is 5 V and the driver signal is a square wave with a 50% duty cycle)

Fig. 10 shows the effect of V_{DS} on R_{on} with different values of V_{GS}. V_{DS} is the device's OFF state voltage. The dotted line is the R_{on} in an ideal state. As V_{DS} exceeds 6 V, R_{on} increases rapidly when V_{GS} is 4 V. However, the resistance is relatively stable when V_{GS} is 5 V. This illustrates that the influence of dynamic R_{on} is more serious when V_{GS} is low.

Two factors affect the dynamic characteristics of the device: V_{DS} and V_{GS}. They affect devices in different states. V_{DS} influences the device in the OFF state. It changes the electric field in the channel, leading to electrons being captured by traps and increasing the value of R_{on}. V_{GS} mainly influences the device in the ON state. High positive V_{GS} can cause the electrons to be easily released from the traps and reduces R_{on}. Therefore, when V_{GS} = 5 V, R_{on} is slightly affected by V_{DS}. In contrast, when V_{GS} is 4 V, increasing V_{DS} leads to a more serious dynamic R_{on} response.

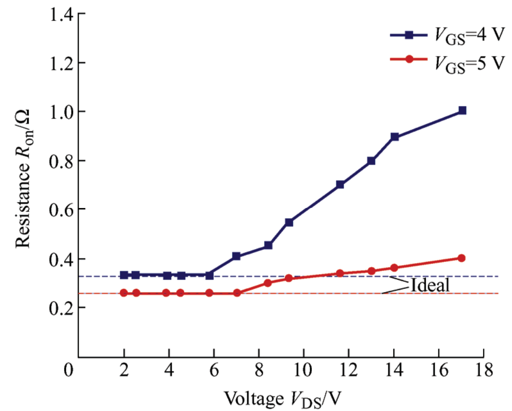

Fig. 10 Relationship between R_{on} and V_{DS} under different gate voltages (The dotted line is R_{on} in the ideal state)

Fig. 11 shows the variation of R_{on} for frequencies between 100 kHz and 1 MHz. For V_{GS} = 4 V, the variation of R_{on} with frequency can be understood as the traps' capture and release. V_{DS} makes the traps capture electrons in the OFF state and V_{GS} makes the traps release electrons in the ON state. With the increase in frequency, a lower V_{GS} cannot immediately make the traps release electrons. When the frequency exceeds 1 MHz, R_{on} is not changed, indicating that the processes of capture and release are balanced. For V_{GS} = 5 V, R_{on} is relatively insensitive to frequency.

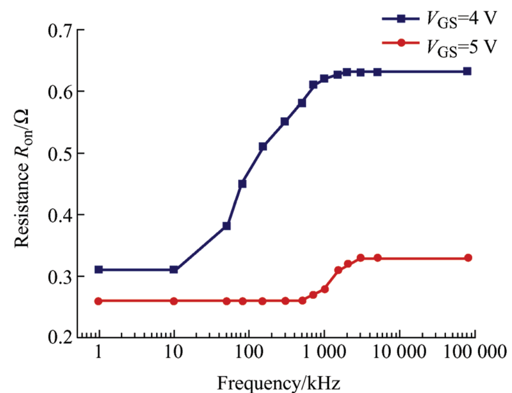

Fig. 11 Relationship between R_{on} and frequency under different gate voltages (The current is 0.25 A and V_{DS} is 10 V)

Because the GaN device does not have a substrate

electrode, Wang et al.[16] reported a test method to determine the effect of the substrate traps. In Fig. 12, $R_{on,D}$ is the resistance R_{on} of the device working at 6.78 MHz and $R_{on,S}$ is the DC value of the device. With the increase in V_{GS}, the ratio $R_{on,D}/R_{on,S}$ decreases and gradually stabilizes, indicating that the traps are in the substrate. For V_{DS} = 20 V, the stable ratio is not 1. We consider that this could be another mechanism for generating dynamic R_{on}.

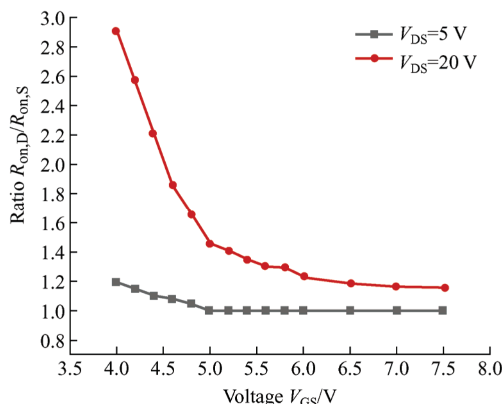

Fig. 12 Change of the dynamic R_{on} under different V_{GS} values (V_{DS} is 20 V and 5 V)

Traps can be created by carbon doping in GaN to increase the insulation of the substrate [17-20]. Many traps were introduced by carbon under the channel. These traps produce the acceptor level in the energy band. When the device turns off, V_{DS} captures the electrons captured by the traps. When the device turns on, V_{GS} releases electrons from the traps.

For the forward mode, the dynamic resistance R_{on} is mainly related to the substrate carbon doping. In addition, the influence of dynamic R_{on} is strongly correlated with V_{GS} and V_{DS}.

4.2 Reverse mode

Two types of reverse modes are illustrated in Fig. 13. Fig. 13a shows the reverse operation mode under ideal conditions of the WPT system (reverse mode I). If the gate drive produces an oscillation and causes the potential between the source and the gate to differ, reverse mode I could change to reverse mode Ⅱ(Fig. 13b). We evaluated the dynamic effects of both reverse modes in an operational condition.

In Fig. 13a, the gate connects to the source and current flows from the source to the drain. The device turns on when $V_{GD} > V_{TH}$. Fig. 14 shows the output characteristics for reverse mode I under the DC test. When V_{SD} exceeds 2.7 V, the device is damaged. We attribute the device damage to the effect of heating.

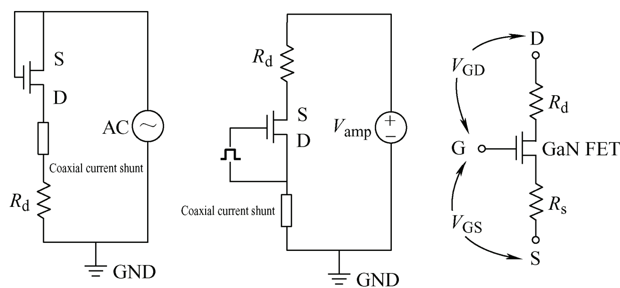

(a) Reverse mode Ⅰ (b) Reverse mode Ⅱ (c) Parastic parameter

Fig. 13 Different operation modes and GaN FET simplified parastic paraneter model

Fig. 15 compares the relationship between R_{on} and current under the forward mode and reverse mode Ⅱ. In reverse mode Ⅱ, R_{on} increases rapidly when the current exceeds 0.3 A. This can be explained by Fig. 13c. Because of the asymmetric design of the device, in general, the gate-source distance is less than the gate-drain distance. This leads to parasitic resistance $R_s < R_d$. Under the same conditions, the high parasitic resistance will reduce the efficiency gate voltage and increase R_{on}. To avoid this influence, we chose the current to be 0.25 A.

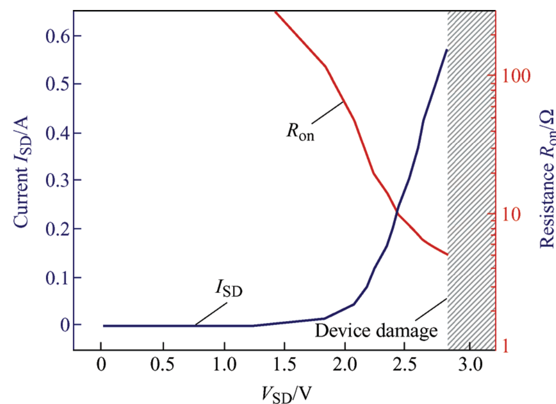

Fig. 14 Device output characteristic under reverse mode I

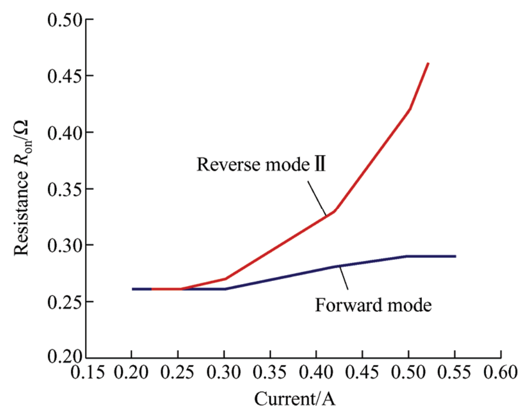

Fig. 15 R_{on} under different currents in a dynamic system (V_{amp}=5 V and the working frequency is 6.78 MHz)

Fig. 16 compares R_{on} for different operation modes. The gate voltage was set to 5 V. The dynamic R_{on} is more obvious when the device operates in reverse mode Ⅱ. We also performed a frequency test as was illustrated in Fig. 11. As can be seen, R_{on} is essentially independent of the frequency. A mechanism can explain this phenomenon. Traps exist between the passivation layer and the barrier layer [21-22]. When the device turns off, the gate injects electrons to the source-side barrier layer and the gate dielectric layer in reverse mode Ⅱ [23]. Electrons are captured at the interface between the source-side barrier and the passivation layer. As the device turns on, gate voltage will extract the electrons from the traps.

In the experiment, the gate driver signal was a 50% duty cycle square wave. The device had the same turn-on and turn-off times. We consider that these two processes, electron injection (OFF state) and extraction (ON state), cancel each other so that R_{on} does not vary with frequency under reverse mode Ⅱ.

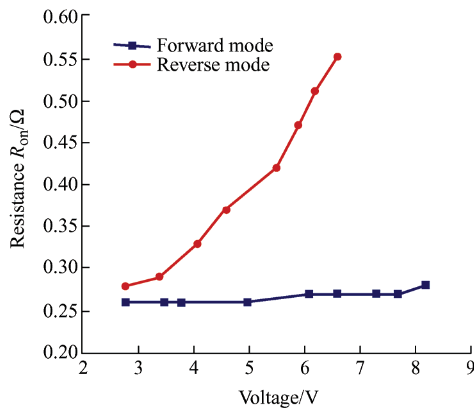

Fig. 16 Dynamic R_{on} under reverse mode Ⅱ and the forward mode (In the forward mode, the X axis is V_{DS}; In reverse mode Ⅱ, the X axis is V_{SD})

Fig. 17 shows the two mechanisms of dynamic R_{on} generation. We studied a commercial GaN transistor (EPC2107), but accurate determination of the mechanism of dynamic R_{on} must rely upon a combination of the device structure and fabrication process.

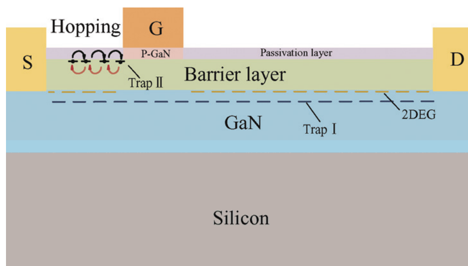

Fig. 17 Schematic of dynamic R_{on} generation mechanism (Two different types of traps produce nonideal effects)

5 Thermal effect

The effect of temperature on R_{on} is shown in Fig. 18. To limit the dynamic R_{on} effect, we set the drain voltage to 10 V in the forward mode. The temperature was controlled by the duty cycle of the square wave, and it was taken on the backside surface of the GaN FET by using an infrared camera.

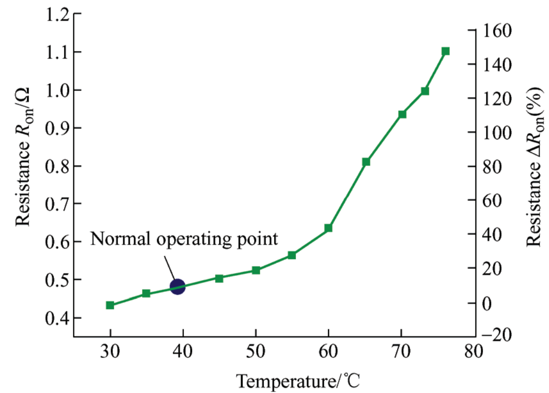

Fig. 18 Effect of temperature on R_{on} (The test circuit is Fig. 8 and V_{GS} = 5 V; The point marks system operation in an ideal condition)

An increase in temperature reduces the mobility of the two-dimensional electron gas, which increases R_{on} [24]. When the temperature rises from 50 ℃ to 70 ℃, R_{on} increases from 0.52 Ω to 0.92 Ω. The device may fail when the temperature rises above 70 ℃ (when R_{on} increases by >100%).

6 Influence of nonideal effects on the circuit

Two nonideal effects, dynamic R_{on} and thermal effects, were studied. In a WPT system, different operation conditions will lead to different nonideal effects becoming the dominant factor in restraining system efficiency.

Clearly, the open-load or high-V_{amp} condition can damage the GaN HEMT in a WPT system. In many cases, the device can fail instantaneously, and we cannot capture the value of R_{on} (such as when V_{DS} = 50 V with no load). We consider that the damage is caused by heat.

In a WPT system, the level of stress on the GaN FET is closely related to the working conditions. For example, when the transmission distance is long, the system will generate a high current flowing through the GaN device, which will produce heat and could even

cause device damage. This effect needs to be addressed at the system level.

7 Conclusions

The impact of the GaN FET R_{on} during operation in a WPT system was studied. Four test methods were compared. Using a coaxial current shunt can most accurately measure dynamic R_{on} in real time in a circuit. Because of the particular operation mode for the WPT system, the dynamic R_{on} device under forward and reverse modes was studied. We found that the traps caused by carbon doping play a major role in the forward mode. The traps located at the interface between the barrier layer and the passivation layer have more influence on the reserve mode. Both trap-induced and heat-induced could cause R_{on} changes, with the latter being more significant at low V_{DS}.

In our research, we found that R_{on} can saturate because of the trap, while heat dissipation tends to increase R_{on} in a positive feedback manner. Therefore, for commercially ready GaN FETs dynamic R_{on} could not be a bottle neck in WPT applications at present.

References

[1] H C Chiu, H L Kao, K S Chin, et al. 6 inch GaN on Si power devices for wireless charged health care system applications. *2015 IEEE MTT-S 2015 International Microwave Workshop Series on RF and Wireless Technologies for Biomedical and Healthcare Applications (IMWS-BIO)*, Taipei, China, 2015: 145-146.

[2] B Ju, H Pan, N Jia, et al. An improved magnetic coupling resonant wireless charging system for cell phones. *PCIM Asia 2018; International Exhibition and Conference for Power Electronics, Intelligent Motion, Renewable Energy and Energy Management*, Shanghai, China, 2018: 1-8.

[3] Y Park, B Jang, S Park, et al. A triple-mode wireless power-receiving unit with 85.5% system efficiency for A4WP, WPC, and PMA applications. *IEEE Transactions on Power Electronics*, 2018, 33(4): 3141-3156.

[4] S Kim, H Abbasizadeh, B S Rikan, et al. A –20 to 30 dBm input power range wireless power system with a MPPT-based reconfigurable 48% efficient RF energy harvester and 82% efficient A4WP wireless power receiver with open-loop delay compensation. *IEEE Transactions on Power Electronics*, 2019, 34(7): 6803-6817.

[5] D Song, F Shi, S Dai, et al. Design and analysis of a wireless power transmission system with magnetic coupling resonance in the weak-coupling region. *Chinese Journal of Electrical Engineering*, 2019, 5(4): 51-60.

[6] T N T Do, A Malmros, P Gamarra, et al. Effects of surface passivation and deposition methods on the 1/*f* noise performance of AlInN/AlN/GaN high electron mobility transistors. *IEEE Electron Device Letters*, 2015, 36(4): 315-317.

[7] W Wang, F Pansier, J Popovic, et al. Design and optimization of a GaN GIT based PFC boost converter. *Chinese Journal of Electrical Engineering*, 2017, 3(3): 34-43.

[8] Q Li, B Liu, S Duan. Simplified analytical model for estimation of switching loss of cascode GaN HEMTs in totem-pole PFC converters. *Chinese Journal of Electrical Engineering*, 2019, 5(3): 1-9.

[9] T Yao, R Ayyanar. A multifunctional double pulse tester for cascode GaN devices. *IEEE Transactions on Industrial Electronics*, 2017, 64(11): 9023-9031.

[10] H Chiu, L Lin. A high-efficiency soft-switched AC/DC converter with current-doubler synchronous rectification. *IEEE Transactions on Industrial Electronics*, 2005, 52(3): 709-718.

[11] A D Koehler, T J Anderson, M J Tadjer, et al. Impact of surface passivation on the dynamic ON-resistance of Proton-irradiated AlGaN/GaN HEMTs. *IEEE Electron Device Letters*, 2016, 37(5): 545-548.

[12] J Bačmaga, R Blečić, R Gillon, et al. Modelling and validation of high-current surface-mount current-sense resistor. *2018 IEEE 22nd Workshop on Signal and Power Integrity (SPI)*, Brest, 2018: 1-4.

[13] Z Liu, X Huang, F C Lee, et al. Package parasitic inductance extraction and simulation model development for the high-voltage cascode GaN HEMT. *IEEE Transactions on Power Electronics*, 2014, 29(4): 1977-1985.

[14] T Soma, S Hori, A Wentzel, et al. A 2-W GaN-based three-level class-D power amplifier with tunable back-off efficiency. *2017 IEEE MTT-S International Microwave Symposium (IMS)*, Honololu, HI, 2017: 2033-2036.

[15] S Huang, J Zhang, W Wu, et al. Impact of non-ideal waveforms on GaN power FET in magnetic resonant wireless power transfer system. *Chinese Journal of Electrical Engineering*, 2019, 5(3): 30-41.

[16] M Wang, D Yan, C Zhang, et al. Investigation of surface- and buffer-induced current collapse in GaN high-electron mobility transistors using a soft switched pulsed *I-V* measurement. *IEEE Electron Device Letters*, 2014, 35(11): 1094-1096.

[17] J T Chen, U Forsberg, E Janzen. Impact of residual carbon on two-dimensional electron gas properties in $Al_xGa_{1-x}N$/GaN heterostructure. *Applied Physics Letters*, 2013, 102(19): 193506.

[18] G Verzellesi, L Morassi, G Meneghesso, et al. Influence of buffer carbon doping on pulse and AC behavior of insulated-gate field-plated power AlGaN/GaN HEMTs. *IEEE Electron Device Letters*, 2014, 35(4): 443-445.

[19] H Yacoub, D Fahle, M Eickelkamp, et al. Effect of stress voltage on the dynamic buffer response of GaN-on-silicon transistors. *Journal of Applied Physics*, 2016, 119(13): 668-670.

[20] C Koller, G Pobegen, C Ostermaier, et al. Effect of carbon doping on charging/discharging dynamics and leakage behavior of carbon-doped GaN. *IEEE Transactions on Electron Devices*, 2018, 65(12): 5314-5321.

[21] D Bin, L Jie, W Ning, et al. Trap behaviours characterization of AlGaN/GaN high electron mobility transistors by room-temperature transient capacitance measurement. *Aip Advances*, 2016, 6(9): 095021.

[22] Y Shi, Q Zhou, W Xiong, et al. Observation of self-recoverable gate degradation in p-GaN AlGaN/GaN HEMTs after long-term forward gate stress: The trapping & detrapping dynamics of hole/electron. *2019 31st International Symposium on Power Semiconductor Devices and ICs (ISPSD)*, Shanghai, China, 2019: 423-426.

[23] L Xia, A Hanson, T Boles, et al. On reverse gate leakage current of GaN high electron mobility transistors on silicon substrate. *Applied Physics Letters*, 2013, 102(11): 1022-1026.

[24] V Volchek, D Dinh Ha, V Stempitsky, et al. Suppression of the self-heating effect in AlGaN/GaN high electron mobility transistor by diamond heat sink layers. *2016 International Conference on Advanced Technologies for Communications (ATC)*, Hanoi, 2016: 264-267.

Shaoyu Sun received his B.S. degree in microelectronics science and engineering from Xidian University, Xi'an, China, in 2018. Since 2018, he has been working toward his M.S. degree at the School of Information Engineering, Peking University of Shenzhen, Shenzhen, China. He has published two academic papers and since 2019 has been studying at Peking University, Beijing, China. His current research interests include GaN devices for advanced radio frequency and power electronics applications.

Jianshan Zhang received his B.S. degree in electrical engineering from Jimei University, Xiamen, China, in 2017. Since 2017, he has been working toward his M.S. degree at the College of Physics and Information Engineering, Fuzhou University, Fuzhou, China. Since 2018, he has been studying at Peking University, Beijing, China, through a joint training program between schools. His current research interests include the design and testing of wireless power transfer systems, GaN, and power electronic devices and applications.

Wengang Wu received his B.S. and Ph.D. degrees in electrical engineering, respectively, from Fudan University, Shanghai, China, and Xi'an Jiaotong University, Xi'an, China. From 1995 to 1997, he worked as a postdoctoral fellow at the Institute of Semiconductors, Chinese Academy of Sciences. From 1997 to 2000, he studied abroad at the University of California, Los Angeles, and became a postdoctoral researcher. His major scientific research works include the preparation of quantum dot superlattices of Si/Ge and III-V group materials and design, fabrication, characteristic tests, and simulation research on high-frequency high-power AlGaN/GaN HEMTs and amplifiers. His current research interests include GaN power electronic devices and micro and nano electromechanical systems technology. He has published more than 200 research papers in first-class international academic journals, in domestic core academic journals, and at internationally important academic conferences. He is now a full professor, doctoral supervisor, and vice-head of the Institute of Micro & Nanoelectronics at Peking University.

Ling Xia received his B.S. and M.S. degrees from Peking University in 2003 and 2006, respectively, and his Ph.D. degree from the Massachusetts Institute of Technology in 2012, all in electrical engineering. He has more than 10 years of experience in compound semiconductor devices and has authored over 20 papers and holds 10 patents in this field. From 2012 to 2013, he was a senior engineer at MACOM Technology Solutions, Inc. From 2013 to 2018, he was with Cambridge Electronics, Inc., working on GaN power electronics. His current research interests include III-V devices for advanced radio frequency and power electronics applications.

Yufeng Jin received his doctoral degree in physical and optical-electronics engineering from Southeast University, China, in 1999. Since then, he has worked as a post-doctoral fellow, associate professor, and professor at Peking University and Peking University, Shenzhen Graduate School. His research interests focus on micro electromechanical systems sensors, TSV-related 3D integration of microsystems, and their application systems. His 3D SiP group has established a close relationship with Intel, Samsung, Simtech, Huawei, SMIC, ASTRI, and CETC on the development of TSV 3D integration technologies.